



Copper-Based Metal–Organic Porous Materials for CO₂ Electrocatalytic Reduction to Alcohols

Jonathan Albo,^{*,[a]} Daniel Vallejo,^[b] Garikoitz Beobide,^[b] Oscar Castillo,^[b] Pedro Castaño,^[a] and Angel Irabien^[c]

The electrocatalytic reduction of CO₂ has been investigated using four Cu-based metal–organic porous materials supported on gas diffusion electrodes, namely, (1) HKUST-1 metal–organic framework (MOF), [Cu₃(μ₆-C₉H₃O₆)₂]_n; (2) CuAdeAce MOF, [Cu₃(μ₃-C₅H₄N₅)₂]_n; (3) CuDTA mesoporous metal–organic aerogel (MOA), [Cu(μ-C₂H₂N₂S₂)]_n; and (4) CuZnDTA MOA, [Cu_{0.6}Zn_{0.4}(μ-C₂H₂N₂S₂)]_n. The electrodes show relatively high surface areas, accessibilities, and exposure of the Cu catalytic centers as well as favorable electrocatalytic CO₂ reduction performance, that is, they have a high efficiency for the produc-

tion of methanol and ethanol in the liquid phase. The maximum cumulative Faradaic efficiencies for CO₂ conversion at HKUST-1-, CuAdeAce-, CuDTA-, and CuZnDTA-based electrodes are 15.9, 1.2, 6, and 9.9%, respectively, at a current density of 10 mA cm⁻², an electrolyte-flow/area ratio of 3 mL min cm⁻², and a gas-flow/area ratio of 20 mL min cm⁻². We can correlate these observations with the structural features of the electrodes. Furthermore, HKUST-1- and CuZnDTA-based electrodes show stable electrocatalytic performance for 17 and 12 h, respectively.

Introduction

The reduction of the CO₂ concentration in the atmosphere has become a critical challenge for sustainable development. There are different approaches to mitigate CO₂ emissions from the use of fossil fuels, including CO₂ capture^[1–3] and subsequent storage or its conversion into valuable chemicals.^[4–6] CO₂ is considered to be a carbon source for the synthesis of valuable chemicals, as it is abundant in the atmosphere and nontoxic compared with the other C₁ source, CO; therefore, the beneficial reuse of CO₂ is an interesting approach for the future. To this end, several methods have been adopted for the conversion and activation of CO₂ such as chemical, thermochemical, photochemical, biochemical, electrochemical, and hydrothermal methods.^[7] Among them, electrocatalytic valorization appears to be a promising strategy owing to its simple procedure and ambient operation conditions. In addition, this technology

coupled to a renewable energy source, such as wind or solar energy, could generate carbon-neutral fuels or industrial chemicals that are derived conventionally from petroleum.^[8] In recent years, many investigators have studied the electrocatalytic reduction of CO₂ on metallic^[9] and modified electrodes in aqueous, nonaqueous, and ionic-liquid media^[10] under different operating conditions and system configurations to produce a range of useful products for industrial chemistry (i.e., formic acid, methane, ethane, ethylene, propylene, methanol, and ethanol). In particular, the challenges for the conversion of CO₂ into high-energy-density alcohols, such as methanol (CH₃OH), are great, but the potential rewards are even greater.^[8,11,12]

Among the different cathode metals applied, Cu uniquely produces hydrocarbons at high reaction rates over sustained periods of time;^[9,13,14] therefore, it is the strongest candidate for CO₂ electrocatalytic reduction. However, Cu generates a range of reaction products, and the selectivity of each product tends to be low.^[15] Thus, to improve the selectivity, other catalyst structures should be considered to make the electrocatalytic reduction of CO₂ at Cu-based surfaces technically and economically viable.

In the last decade, metal–organic porous materials (MOPMs) and, particularly, metal–organic frameworks (MOFs), also known as porous coordination polymers or porous coordination networks, have shown many potential applications as new multifunctional materials. MOFs are hybrid materials containing three well-differentiated sites to which the catalytic function can be allocated, namely, the metallic component, the organic linker, and the pore space. MOFs are considered as ideal candidates for CO₂ adsorption, separation,^[16] and reduction through catalyzed reactions.^[17] This is because of their combined favor-

[a] J. Albo, P. Castaño

Department of Chemical Engineering
University of the Basque Country (UPV/EHU)
PO Box. 644, 48080, Bilbao (Spain)
E-mail: jonathan.albo@ehu.es

[b] D. Vallejo, G. Beobide, O. Castillo

Department of Inorganic Chemistry
University of the Basque Country (UPV/EHU)
PO Box. 644, 48080, Bilbao (Spain)

[c] A. Irabien

Department of Chemical & Biomolecular Engineering
University of Cantabria (UC)
Avda. Los Castros, 39005, Santander (Spain)

Supporting information and the ORCID identification number(s) for the author(s) of this article can be found under <http://dx.doi.org/10.1002/cssc.201600693>.

This publication is part of a Special Issue around the “1st Carbon Dioxide Conversion Catalysis” (CDCC-1) conference. A link to the issue's Table of Contents will appear here once it is complete.

able properties of large surface area, high porosity, tunable pore-size, and shape-selective character. Indeed, MOFs are particularly suitable for electrochemical reactions as a result of these features in addition to their high electronic conductivities.^[18–26] For example, Kumar et al.^[19] studied the electrocatalytic reduction of CO₂ on Cu-based MOF (HKUST-1) films with an electrolyte consisting of a DMF solution of tetrabutylammonium tetrafluoroborate saturated with CO₂. Cyclic voltammetry revealed that the electrochemically generated Cu^I species were very selective for CO₂ reduction, although the main product was oxalic acid. In the same year, Hinogami et al.^[20] synthesized a copper rubeanate MOF (CR-MOF) supported on carbon films as electrodes. The onset potential for CO₂ reduction at the CR-MOF electrode was approximately 0.20 V higher than that observed on a Cu metal electrode. Hod et al.^[23] synthesized iron-porphyrin-based MOFs for the electrocatalytic conversion of CO₂; these materials exhibited high active-site exposure ($\approx 10^{15}$ sites per cm²) and nearly 100% Faradaic efficiency (FE) for the production of CO + H₂ mixtures. Kornienko et al.^[24] obtained 76% Faradaic efficiency and high stability for 7 h using Co-porphyrin MOFs. On the contrary, examples of metal-organic aerogels (MOAs) are relatively scarce^[27–31] compared with the more conventional MOFs. To the best of our knowledge, no studies have dealt with their use as electrocatalysts for CO₂ reduction.

To face the challenge of synthesizing effective and stable CO₂ reduction electrocatalysts for the continuous production of alcohols, in this work, we have evaluated four MOPMs (two MOFs and two MOAs) containing Cu (Figure 1) as gas diffusion electrodes (GDEs), which are named hereafter MOPM-GDEs: (1) a benchmark MOF with formula [Cu₃(μ₆-C₉H₃O₆)₂(OH)₂]_n (C₉H₃O₆ = benzene-1,3,5-tricarboxylate), commonly known as MOF-199 or HKUST-1,^[32] in which the accessible metallic moieties are adsorption sites for CO₂,^[33] (2) a microporous copper(II)-adeninate-acetate coordination framework with formula [Cu₂(μ₃-adeninate)₂(μ₂-OOC(CH₃)₂)_n·xH₂O (CuAdeAce), in which the Watson-Crick faces of the adenine are sites for CO₂ adsorption,^[34] (3) a Cu MOA built from successive junctions with bis-bidentate dithiooxamidate (DTA) and named CuDTA; and (4) a MOA with the same synthetic premise as (3) but with oxides of Cu and Zn, named CuZnDTA. The coordination frameworks of MOAs lack intrinsic pore systems; therefore, we have processed the materials as nanofibrous aerogels to increase their surface areas and the accessibility of the catalytic centers. Each MOPM was deposited on a gas diffusion layer to form a characteristic gas-solid-liquid three-phase interface, which allows the mass-transfer limitations usually found in electrochemical systems to be overcome to enhance the CO₂ reduction performance.^[4] Then, we characterized the GDEs through a set of analytical techniques and cyclic-voltammetry analyses and finally tested the materials in the electrocatalytic reduction of CO₂ using a continuous filter-press electrochemical cell under different operating conditions.

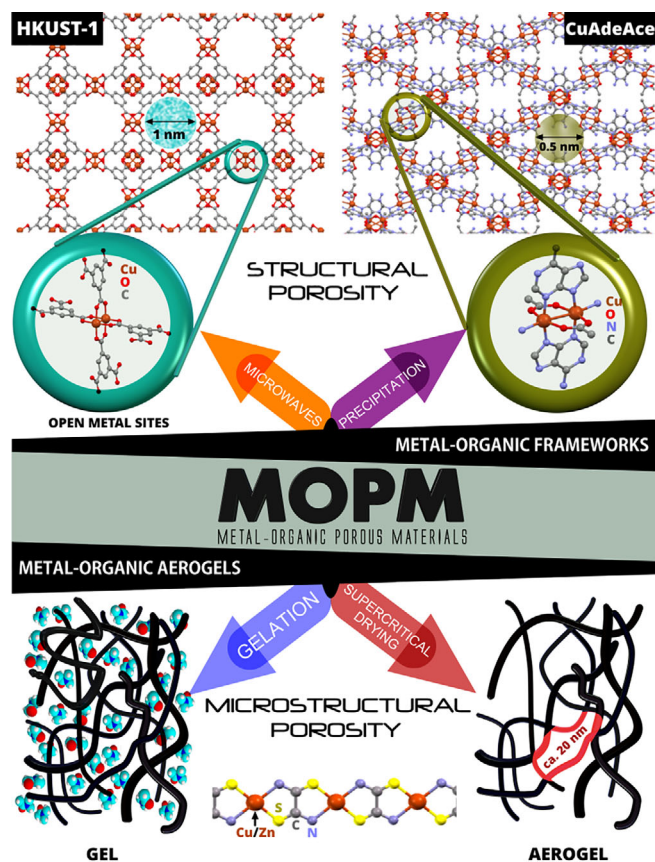


Figure 1. Structural details of the selected metal-organic porous materials (MOPMs).

Results and Discussion

Surface characterization of the GDEs

The MOPM-GDEs were characterized by SEM, attenuated total reflectance (ATR) FTIR spectroscopy, and PXRD to understand their structural and morphological properties in relation to their capability for CO₂ electrocatalytic reduction. In all cases, the SEM images recorded at low magnification (5000×, see Figure S3.1 of the Supporting Information) show that homogeneous films cover the entire sprayed GDE surface. At high magnification (25 000×), the microstructures of the HKUST-1 and CuAdeAce GDEs reveal their polycrystalline natures (Figure 2a and b) with strongly aggregated sub-micrometric crystals and micrometric octahedral crystals, respectively. The images of the CuDTA and CuZnDTA GDEs (Figure 2c and d) reveal filamentous structures composed of highly crosslinked fibers with diameters of 5 to 20 nm, comparable to those of the corresponding as-prepared materials.

All of the ATR-FTIR spectra feature a set of peaks at $\tilde{\nu} = 1305$, 1210, 1150, 1060, and 975 cm⁻¹, which corresponds to the anti-symmetric and symmetric stretching of the sulfonate, perfluorinated, and ether groups of the tetrafluoroethylene copolymer used as the surfactant (Nafion®). Although the MOPMs show less-intense peaks overlapped with those of the surfactant in the low-energy range, the peaks arising from the coordination framework can be distinguished at higher wavenumbers ($\tilde{\nu} = 1310$ –1700 cm⁻¹). The detailed spectroscopy of the MOPM-

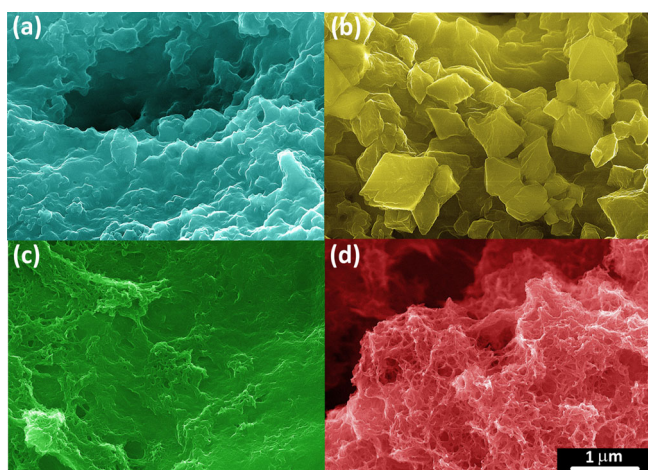


Figure 2. SEM images at 25 000 \times magnification of (a) HKUST-1, (b) CuAdeAce, (c) CuDTA, and (d) CuZnDTA; not real colors.

GDEs and the analysis of the main vibration modes are provided in the Supporting Information (see Figure S3.3 and Table S3.1).

As the performance of a MOF is closely related to its crystallinity, HKUST-1 and CuAdeAce GDEs were further characterized by PXRD (Figure 3). Both MOF-GDEs show characteristic (002) and (004) reflections of the graphite sites at $2\theta = 26.5$ and 54.6° , respectively. Although, the preferred orientation of graphite gives rise to an oversized peak, the signals corresponding to the MOFs are clearly distinguishable at $2\theta < 22^\circ$. As shown in the inset graphic, all of the observed peaks fit the expected lattice-plane reflections.

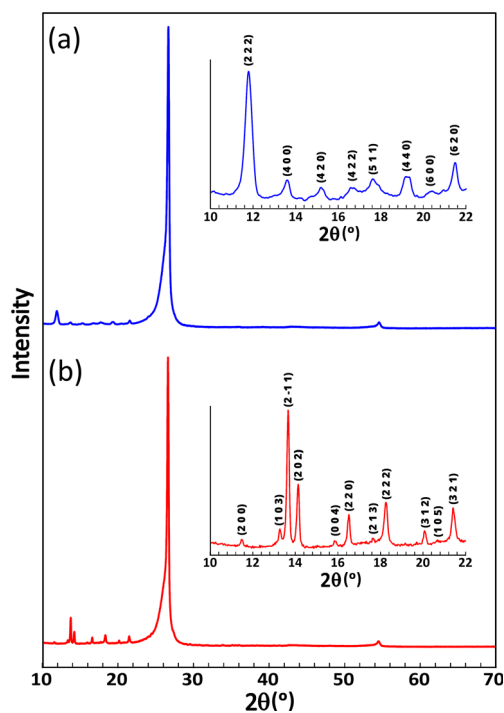


Figure 3. PXRD patterns of HKUST-1 and CuAdeAce GDEs.

Cyclic-voltammetry characterization

To examine the electrocatalytic behavior of the prepared GDEs, cyclic voltammetry was performed for the MOPM-GDEs in CO_2 -saturated (0.5 M KHCO_3) aqueous solutions; the voltammograms after five scans with the current densities (j) normalized to the geometric area of the MOPM-GDEs are shown in Figure 4. The results are compared to the current–voltage response of a Cu plate.

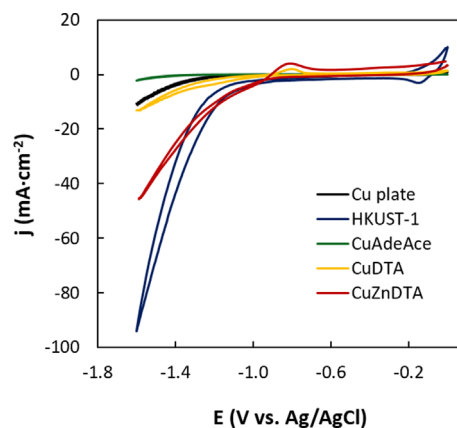


Figure 4. Cyclic voltammograms for the MOPM-GDEs in a CO_2 -saturated 0.5 M KHCO_3 aqueous solution.

Large differences between the voltammetric profiles of the MOPM-GDEs can be seen in Figure 4, and HKUST-1 and CuZnDTA are the most promising candidates for the electroreduction process. All of the voltammetric profiles show a reduction process that starts at approximately -1 V versus Ag/AgCl and is associated with the reduction of CO_2 . On the other hand, for the applied voltage, the CuAdeAce GDE shows almost no response variation, which reveals a low activity for conducting electrons. It is also important to note the synergic effect of Cu and Zn in the reduction response, as denoted by the remarkably lower current densities at lower onset potentials for CuZnDTA compared with those of CuDTA. This result is in agreement with those for $\text{Cu}_2\text{O}/\text{ZnO}$ and Cu_2O GDEs.^[5] Furthermore, the oxidative peak at -0.8 V , previously assigned to the transformation of Zn to ZnO ,^[5] is assigned in this work to the formation of oxidized subproducts from the CO_2 reduction reaction because it is present for both CuDTA and CuZnDTA GDEs, and each voltammetry profile shown in Figure 5 corresponds to the fifth cycle.

To further confirm the reduction of CO_2 , the voltammetry profiles of the most promising GDEs (HKUST-1 and CuZnDTA) in the presence and absence of CO_2 (in an Ar-saturated solution) are shown in Figure 5a and 5b. The decrease of the current intensity for both GDEs is an indication that CO_2 is reduced at an onset potential lower than -1 V versus Ag/AgCl. Thus, the intrinsic oxidation–reduction of the GDEs might be neglected, particularly for HKUST-1 GDE, for which the reduction response in the absence of CO_2 is close to the response for a Cu plate in a CO_2 -saturated KHCO_3 aqueous solution.

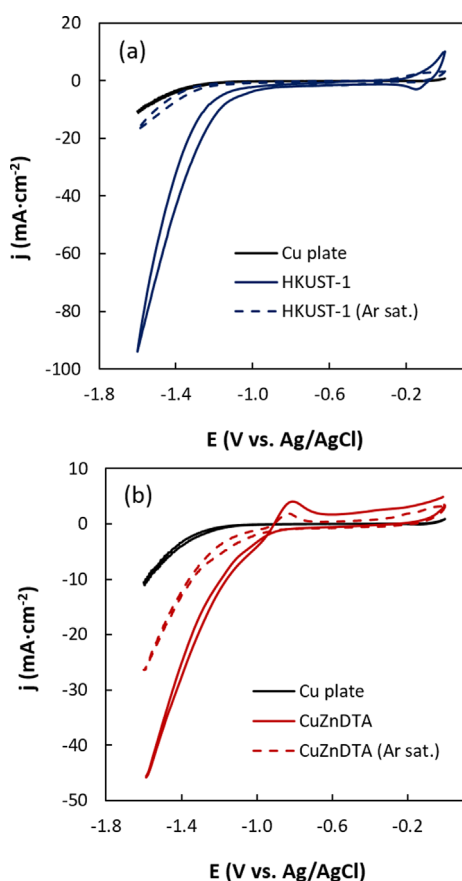


Figure 5. Cyclic-voltammetry responses in medium saturated with CO_2 (0.5 M KHCO_3) and Ar of (a) HKUST-1 and (b) CuZnDTA.

Influence of current density on CO_2 reduction performance

The results for the continuous electrocatalytic reduction of CO_2 in a filter-press electrochemical cell are presented hereafter. The quantitative reduction performances (production rate, r , and Faradaic efficiency, FE) regarding the liquid-phase product distribution at different current densities ($j = 5\text{--}40 \text{ mA cm}^{-2}$) are shown in Figure 6 for the prepared MOPM-GDEs. The electrocatalytic reduction of CO_2 with the MOPM-GDEs leads to the formation of CH_3OH and $\text{C}_2\text{H}_5\text{OH}$. It should be noted that the carbon paper without MOPMs did not produce any measurable liquid product. The FEs were calculated for a 6-electron pathway for CO_2 reduction to CH_3OH and a 12-electron pathway to $\text{C}_2\text{H}_5\text{OH}$. A constant electrolyte-flow/area ratio (Q_e/A) and gas-flow/area ratio (Q_g/A) of 2 and $20 \text{ mL min}^{-1} \text{ cm}^{-2}$, respectively, were applied. These conditions were found previously to be optimal for the electrocatalytic reduction of CO_2 .^[4]

As shown in Figure 6, the product distribution and process efficiency are correlated with the current density applied to the system. The HKUST-1 and CuZnDTA GDEs are the most active electrocatalysts for the reduction of CO_2 , in agreement with the higher reduction responses observed in the cyclic-

voltammetry profiles (Figure 4). This electrocatalytic performance is partially correlated with the surface area of the GDEs, as summarized in Table S2.1 in the Supporting Information: the HKUST-1 GDE exhibits the highest surface area ($1710 \text{ m}^2 \text{ g}^{-1}$) and the highest electrocatalytic performance, whereas CuDTA and CuZnDTA GDEs exhibit much lower surface areas (270 and $260 \text{ m}^2 \text{ g}^{-1}$, respectively) and significantly poorer electrocatalytic performances. Nevertheless, the surface area is not the only parameter that controls the catalytic performance, as CuAdeAce GDE with an intermediate area ($500 \text{ m}^2 \text{ g}^{-1}$) shows the lowest FE values. The last results could be anticipated from the cyclic-voltammetry profiles displayed in Figure 4, which indicated the lowest electron conductivity for the CuAdeAce GDE. Thus, the electrocatalytic performance should be related to additional features of the GDEs that require additional analysis of the Cu active sites, particularly the accessibility of the pentacoordinate Cu^{II} centers, which are hindered sterically by the surrounding ligands. This leads to the preliminary conclusion that MOPMs with unsaturated coordination positions exposed in the pore system are preferred for the enhancement of the performance of the electrocatalytic reduction of CO_2 to alcohols.

The maximum CH_3OH and $\text{C}_2\text{H}_5\text{OH}$ production rates for the HKUST-1 GDEs ($r_{\text{CH}_3\text{OH}} = 5.62 \times 10^{-6} \text{ mol m}^{-2} \text{ s}^{-1}$ and $r_{\text{C}_2\text{H}_5\text{OH}} = 5.28 \times 10^{-6} \text{ mol m}^{-2} \text{ s}^{-1}$) correspond to product concentrations in the catholyte of 0.54 and 0.73 mg L^{-1} for CH_3OH and $\text{C}_2\text{H}_5\text{OH}$, respectively. The formation of both alcohols, CH_3OH and $\text{C}_2\text{H}_5\text{OH}$, has been reported previously,^[4,15,35–46] whereas Cu-based GDEs are more selective towards the formation of CH_3OH over $\text{C}_2\text{H}_5\text{OH}$.^[4] The maximum FEs of CH_3OH and $\text{C}_2\text{H}_5\text{OH}$ were 54.8 and 31.4% for Cu_2O and $\text{Cu}_2\text{O}/\text{ZnO}$ GDEs, respectively, at applied potentials of -1.39 and -1.16 V versus Ag/AgCl .^[4] Furthermore, the CuO GDE led to a higher selectivi-

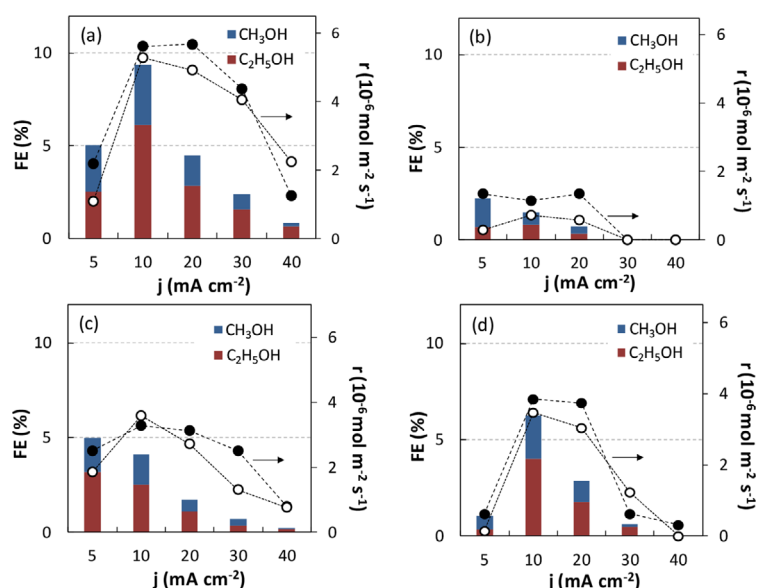


Figure 6. Rates (r) for CH_3OH (●) and $\text{C}_2\text{H}_5\text{OH}$ (○) formation and Faradaic efficiencies (FEs) in the electrocatalytic reduction of CO_2 as a function of the current density (j) applied with (a) HKUST-1, (b) CuAdeAce, (c) CuDTA, and (d) CuZnDTA; the lines are only guides.

ty for C_2H_5OH (FE = 15.5%) in a 0.2 M $KHCO_3$ solution,^[39] and trace amounts of CH_3OH and C_3H_8O were also detected. Another example is the recent study conducted by Gutierrez-Guerra et al.^[46] for different Cu-based GDEs, which afforded CH_3OH and C_2H_5OH with selectivities of 80 and 10%, respectively, at an applied current of -30 mA. Kuhl et al.^[15] reported a total of 16 different CO_2 reduction products (including CH_3OH and C_2H_5OH) across a range of potentials. They hypothesized that the chemistry involved in the C–C coupling reactions to form C_2 – C_3 products occurs through an enol-like surface intermediate, which desorbs to convert to its diol or ketone form. Certainly, the C–C bond formation is one of the most critical factors to be considered in the design of electrocatalysts for the production of alcohols, and further experimental work is needed to fully elucidate the CO_2 reduction steps to form alcohols using Cu-based GDEs.

As shown in Figure 6, the rates for CO_2 reduction to CH_3OH and C_2H_5OH did not improve at $j > 10$ mA cm^{-2} . At this point, the maximum r values can be obtained for all MOPM-GDEs. The total Faradaic efficiency (FE_T, cumulative efficiency for the formation of CH_3OH and C_2H_5OH) drops drastically as the current increases from $j = 10$ to 40 mA cm^{-2} . This result could be explained by the consumption of the additional current by side reactions; hence, the optimal current density is 10 mA cm^{-2} for all MOPM-GDEs. Under these conditions, the FE_T values are 10.9 and 7.3% for the HKUST-1 and CuZnDTA GDEs, respectively. The remaining product is expected to be mainly H_2 , which competes with the electrocatalytic reduction of CO_2 to alcohols and affects the GDE stability negatively. The latter observation is caused by the fact that H_2 favors the leaching of the active material from the GDE.^[4]

Influence of electrolyte flow rate and gas flow rate

Previous studies demonstrated that variations in Q_e and Q_g could lead to significant mass-transfer differences in the cell and, thus, in the total rate for CO_2 transformation, r_T , and the cumulative FE_T of the process.^[4,5] These effects can be observed even for the application of GDEs,^[4] for which mass-transfer limitations are expected to be overcome partially.^[6,47,48]

In an attempt to improve the CO_2 conversion efficiency, additional experiments were conducted at different Q_e/A and Q_g/A values. The results are presented in Figure 7. The increase in Q_e/A from 1 to 3 mL $min^{-1} cm^{-2}$ led to a significant enhancement in the CO_2 electrocatalytic conversion rate (Figure 7a, e.g., from $r_T = 5.80 \times 10^{-6}$ to 18.57×10^{-6} mol $m^{-2} s^{-1}$ for HKUST-1 GDE). The use of low Q_e/A ratios is preferred as the concentration of alcohols in the liquid would be higher; therefore, for an optimal process operation, a compromise needs to be met between the concentration of alcohols in the product and their formation rate. Further increases in Q_e/A led to a drastic decrease in r_T owing to the leaching of the active material from the GDE.^[4] Furthermore, a low Q_e/A allows the infiltration of the catholyte into the GDE structure, which increases the diffusion time and enhances CO_2 electrocatalytic performance.^[4,48,49]

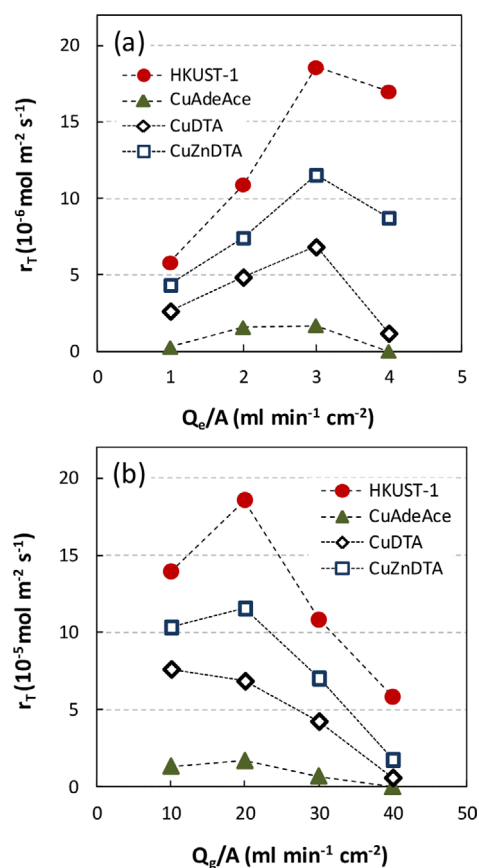


Figure 7. Total rates (r_T) at $j = 10$ mA cm^{-2} for the MOPM-GDE with (a) different electrolyte flow rates (Q_e/A) and (b) CO_2 gas flow rates (Q_g/A); the lines are only guides.

Moreover, the increases in Q_g/A from 10 to 20 mL $min^{-1} cm^{-2}$ yields an increase of the CO_2 electrocatalytic conversion rate (Figure 7b, e.g., from $r_T = 13.94 \times 10^{-6}$ to 18.57×10^{-6} mol $m^{-2} s^{-1}$ for HKUST-1 GDE). This observation reveals that the overall kinetics at $Q_g/A = 10$ mL min^{-1} are controlled by the external transport of CO_2 to the GDE active sites. A further increase of Q_g/A above 20 mL $min^{-1} cm^{-2}$ leads to a drastic decrease in r_T which is then attributed to the leaching of active material from the GDE, in agreement with previous findings.^[4,48,50] Thus, the optimal balance point is at $Q_g/A = 20$ mL $min^{-1} cm^{-2}$, at which enough CO_2 gas supply is provided for the reaction well before a massive detachment of active material occurs.

Overall, the optimal conditions for the CO_2 electrocatalytic reduction on MOPM-GDEs is $Q_e/A = 3$ mL $min^{-1} cm^{-2}$ and $Q_g/A = 20$ mL $min^{-1} cm^{-2}$. The optimal electrocatalytic performances, in terms of r and FE, for the MOPM-GDEs are shown in Table 1. To interpret the electrocatalytic activity further, the total formation rates were normalized to the active Cu surface area of each GDE, $r_{T,a}$. The active Cu area (a) was measured through pulse chemisorption, as described in the Experimental Section. The results were compared to those obtained for a filter-press electrochemical cell equipped with a Cu plate at an applied potential of -1.3 V versus Ag/AgCl ($j = 10.83$ mA cm^{-2}).

Table 1. r and FE for the electrocatalytic conversion of CO_2 at MOPM-GDEs. $j = 10 \text{ mA cm}^{-2}$, $Q_d/A = 3 \text{ mL min}^{-1} \text{ cm}^{-2}$, $Q_g/A = 20 \text{ mL min}^{-1} \text{ cm}^{-2}$.									
GDE	E [V]	a_{Cu} [cm^2]	r [$10^{-6} \text{ mol m}^{-2} \text{ s}^{-1}$]				FE [%]		
			$r_{\text{CH}_3\text{OH}}$	$r_{\text{C}_2\text{H}_5\text{OH}}$	r_{T}	$r_{\text{T},a}$	$\text{FE}_{\text{CH}_3\text{OH}}$	$\text{FE}_{\text{C}_2\text{H}_5\text{OH}}$	FE_{T}
HKUST-1	-0.9	66.48	9.68	8.90	18.58	0.28	5.6	10.3	15.9
CuAdeAce	-1.75	0.13	1.25	0.43	1.68	13.1	0.7	0.5	1.2
CuDTA	-1.41	53.69	3.28	3.58	6.86	0.13	1.9	4.1	6
CuZnDTA	-1.25	1.78	5.93	5.64	11.57	6.52	3.4	6.5	9.9
Cu plate ^[a]	-1.3	-	8.7	-	8.7	-	4.6	-	4.6

[a] Data from Ref. [5] at $j = 10.83 \text{ mA cm}^{-2}$ and $Q_d/A = 2 \text{ mL min}^{-1} \text{ cm}^{-2}$.

The alcohol formation rate after 90 min on-stream varied from $r_{\text{T}} = 1.68 \times 10^{-6}$ to $18.58 \times 10^{-6} \text{ mol m}^{-2} \text{ s}^{-1}$ for CuAdeAce and HKUST-1 GDEs, respectively. The latter GDE also displays the highest FE ($\approx 16\%$) among the studied electrodes. These values, together with those obtained for CuZnDTA GDE, are remarkably greater than those for a Cu plate and show the great opportunities brought by MOPMs for the electrocatalytic reduction of CO_2 . This enhanced performance is related to the demonstrated higher activity for the reduction of protons by CuO_x in comparison with that of Cu^0 for the electrocatalytic reduction of CO_2 .^[24,35-37,51,52] For example, Lan et al.^[37] investigated the electrocatalytic reduction of CO_2 at a Cu/CuO (core-shell) catalyst in 1 M KHCO_3 with a flow reactor. This study proved that transformations between Cu, Cu^{I} , and CuO occurred as a function of applied potential, which at the same time did not affect CH_3OH production severely. Thus, the high yield of CH_3OH obtained at -1.72 V versus Ag/AgCl using a Cu/CuO (core-shell) electrocatalyst was higher than that obtained using Cu foil. Furthermore, the formation rates reached using the HKUST-1 GDEs are in the range of those values reported previously for air-oxidized Cu foil and electrochemically oxidized Cu foil ($r \approx 2 \times 10^{-5} \text{ mol m}^{-2} \text{ s}^{-1}$) at potentials of -1.2 to -1.5 V versus Ag/AgCl.^[53] Nevertheless, the formation rates are still below those reported for Cu_2O GDEs ($r_{\text{T}} = 11.9 \times 10^{-5} \text{ mol m}^{-2} \text{ s}^{-1}$ at -1.05 V versus Ag/AgCl)^[54] and also those achieved with $\text{Cu}_2\text{O}/\text{Zn}$ -based GDEs ($r = 4.74 \times 10^{-5} \text{ mol m}^{-2} \text{ s}^{-1}$).^[4] This result is related to the beneficial properties of Cu^{I} for CO_2 electrocatalytic reduction processes. Previous studies demonstrated that Cu^{I} presents both intermediate hydrogen overpotentials and CO adsorption properties, which promote CO_2 reduction in aqueous solutions in comparison with Cu^0 or Cu^{II} -based electrocatalysts.^[36,51]

Interestingly, if the formation rates are normalized to the active Cu surface available, CuAdeAce shows the highest activity ($r_{\text{T},a} = 13.1 \times 10^{-6} \text{ mol m}^{-2} \text{ s}^{-1}$). Conversely, the lowest rates were observed for the HKUST-1 GDEs ($r_{\text{T},a} = 0.28 \times 10^{-6} \text{ mol m}^{-2} \text{ s}^{-1}$). To explain such unexpected behavior, first it must be considered that the idealized crystal structure suggests that the coordination framework of CuAdeAce lacks accessible unsaturated Cu^{II} coordination positions, and this leads to a low Cu active-surface value ($0.13 \text{ cm}^2 \text{ g}_{\text{Cu}}^{-1}$), which is probably attributable to the presence of crystal defects that render some Cu^{II} sites unhindered and available for N_2O chemisorption. Therefore, the superior value of the normalized rate

found for CuAdeAce implies that the scarce amount of accessible Cu^{II} sites are highly active centers and it provides a clue for the design of more efficient electrocatalysts for CO_2 reduction based on $\{\text{Cu}_2(\mu_3\text{-adeninate})_2[\mu_2\text{-OOC}(\text{CH}_3)_2]\}_n$ paddlewheel motifs.

On the other hand, the comparison of the normalized rates for CuDTA and CuZnDTA (0.13 and $6.52 \text{ mol m}^{-2} \text{ s}^{-1}$) supports the previously inferred crucial role that Zn^{II} centers play on the performance of MOF-GDEs.

Long-term stability of MOPM-GDEs

Finally, the stabilities of the MOPM-GDEs were tested over an extended period. The evolution of the cumulative Faradaic efficiency over 5 h on-stream, FE_{T} , for the observed optimal experimental conditions is shown in Figure 8.

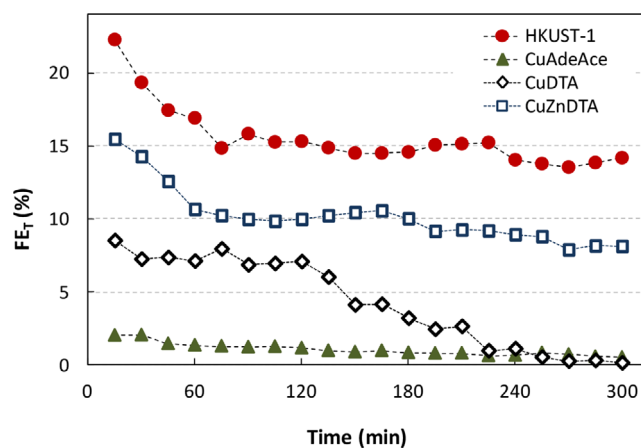


Figure 8. Time-dependence of FE for the MOPM-GDEs under the following conditions: $j = 10 \text{ mA cm}^{-2}$, $Q_d/A = 3 \text{ mL min}^{-1} \text{ cm}^{-2}$, and $Q_g/A = 20 \text{ mL min}^{-1} \text{ cm}^{-2}$; the lines are only guides.

As indicated in Figure 8, during the first minutes of the experiment, the electrolyte needs to diffuse through the internal structure of the GDE to form a typical three-phase interface throughout the whole GDE and, thus, enlarge the contact area.^[55] The electrocatalytic activity (FE_{T}) decays to a plateau and remains almost stable during the rest of the run (pseudostationary state), except that for the CuDTA GDE, which drops to zero after 120 min. This deactivation observed for all MOPM-GDEs is attributed to the decrease of their active-site areas^[48,49] or the degradation of the MOPMs owing to their limited stabilities in water, in which they undergo hydrolysis, amorphization, or phase transformations, even at room temperature.^[56,57] In this sense, the MOPM-GDEs used for 30 min were analyzed further and compared with the as-prepared ones. The ATR-FTIR spectroscopy measurements (Figure 9a and b) of the MOF-GDEs (HKUST-1 and CuAdeAce) show a depletion of the intensity of the main reference signal attributed to the MOF-GDE; this suggests that a degradation of the material occurs during the run.

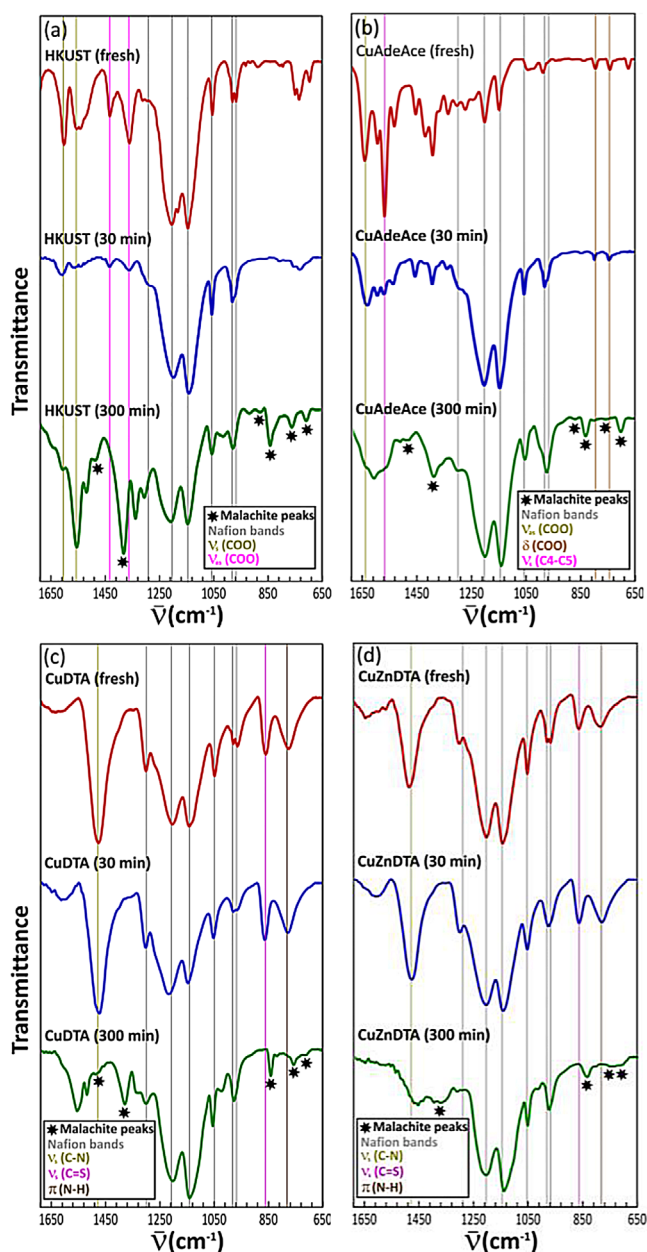


Figure 9. ATR-FTIR spectra for fresh and used (a) HKUST-1, (b) CuAdeAce, (c) CuDTA, and (d) CuZnDTA.

Accordingly, the PXRD analysis of the HKUST-1 and CuAdeAce GDEs (Figure 10) shows a significant reduction of crystallinity, which is more acute for HKUST-1. It must be pointed out that the performance loss of HKUST-1 is smaller than that expected from the drastic crystallinity loss; thus, the remaining efficiency level can be attributed to the preservation of the local structure, as suggested by the FTIR spectra. Coming back to the FTIR analysis (Figure 9), the loss of intensity for the MOA-GDEs (Figure 9c and 9d) is not so evident; therefore, the initial FE_T decay can be related to a shallow surface degradation/modification of the CuDTA and CuZnDTA nanofibers that is not detectable in the FTIR spectra at this stage, as the bulk of the material remains unaltered. However, in all cases, the

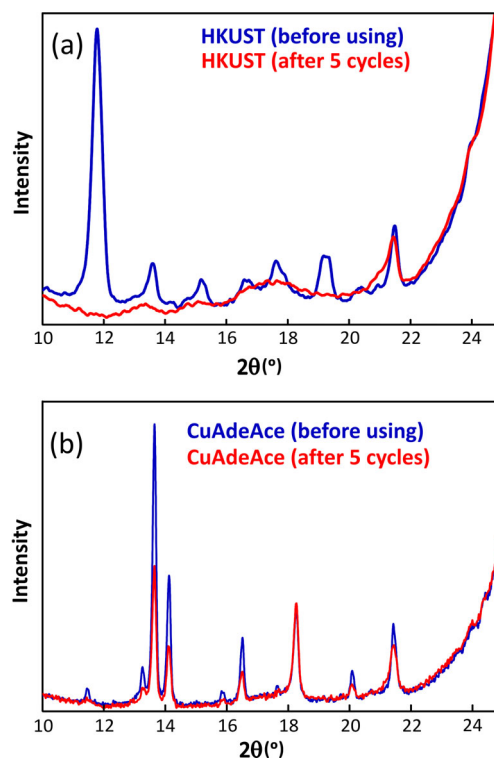


Figure 10. Comparison of the PXRD patterns of fresh and used (a) HKUST-1 and (b) CuAdeAce.

FTIR spectra recorded at the end of the run (300 min, see Supporting Information) reveal a series of emerging peaks that evidence the formation of copper(II) hydroxycarbonate (malachite), which is a plausible degradation path for all Cu-MOPMs and not detectable at the middle of the run. Furthermore, at the end of the run, the decay of the signals corresponding to CuDTA is greater than that observed for CuZnDTA, and this explains the differences in the FE_T trend at the last part of the run.

The FTIR and PXRD analyses of the fresh and used MOPM-GDEs give a qualitative clue to the activity loss, whereas a quantitative one is obtained from the relative FE_T losses. After 5 h on-stream, the relative FE_T drops are 40, 65, 98, and 51% for HKUST-1, CuAdeAce, CuDTA, and CuZnDTA GDEs, respectively. These relative activity losses indicate that all MOPM-GDEs (except CuDTA) retain an intermediate efficiency despite the cited long-term degradation. In a practical sense, a third reason for the deactivation should be indicated, namely the leaching of the MOPM from the rest of the GDE structure (carbon support).^[4] In addition, the probable agglomeration of particles and defects in the catalytic layer during the preparation of the MOPM-GDE would likely assist tunneling and increase the unwanted H_2 formation owing to the easy access of water to catalytic sites.^[51] On the contrary, the GDEs containing HKUST-1 and CuZnDTA are able to retain moderate formation rates (HKUST-1, $r_T = 18.58 \times 10^{-6} \text{ mol m}^{-2} \text{ s}^{-1}$; CuZnDTA, $r_T = 11.57 \times 10^{-6} \text{ mol m}^{-2} \text{ s}^{-1}$) and Faradaic efficiencies (HKUST-1, $FE_T = 15.9\%$; CuZnDTA, $FE_T = 9.9\%$) for as long as 12 or 17 h

and surpass the stability value reached recently for MOF-GDEs for the electrocatalytic transformation of CO₂.^[19]

These results make the use of MOPMs valuable for the CO₂ electrocatalytic conversion to alcohols in continuous operation, although further work is required to design materials with the same favorable properties and a higher stability for a technoeconomically viable CO₂ valorization process. The outstanding challenges remain in the design of catalyst systems featuring (1) selectivity for CO₂ reduction with minimum H₂ generation, (2) high conversion efficiency at low electrochemical overpotentials, and (3) long-term stability. Furthermore, the detailed mechanisms for the overall catalytic system remain unclear. We hope to elucidate the reactions steps for CO₂ conversion to value-added products on MOPM-GDEs.

Conclusions

This work demonstrates the ability of Cu-containing metal-organic porous materials (MOPMs) supported in gas diffusion electrodes (GDEs) to promote the electrocatalytic conversion of CO₂ to alcohols. We successfully prepared, characterized, and tested four different MOPM-GDEs. Specifically, two metal-organic frameworks, (1) [Cu₃(μ₃-C₉H₃O₆)₂]_n (HKUST-1) and (2) [Cu₃(μ₃-C₅H₄N₅)₂]_n (CuAdeAce), and two metal-organic aerogels, (3) [Cu(μ-C₂H₂N₂S₂)]_n (CuDTA) and (4) [Cu_{0.6}Zn_{0.4}(μ-C₂H₂N₂S₂)]_n (CuZnDTA). The characterization involved structural and cyclic-voltammetry analyses, whereas the testing during the electrocatalytic reduction of CO₂ was performed in a continuous setup consisting of a filter-press electrochemical cell under ambient conditions.

The analyses of the electrolysis products showed that methanol and ethanol were formed predominately as the liquid products from CO₂ reduction. An enhanced performance for CO₂ conversion was achieved through the application of HKUST-1 and CuZnDTA GDEs at a current density (*j*) of 10 mA cm⁻², an electrolyte-flow/area ratio (*Q_e/A*) of 3 mL min⁻¹ cm⁻², and a gas-flow/area ratio (*Q_g/A*) of 20 mL min⁻¹ cm⁻², at which moderate formation rates (KHUST-1, *r_T* = 18.58 × 10⁻⁶ mol m⁻² s⁻¹; CuZnDTA, *r_T* = 11.57 × 10⁻⁶ mol m⁻² s⁻¹) and Faradaic efficiencies (KHUST-1, FE_T = 15.9%; CuZnDTA, FE_T = 9.9%) could be obtained. These results denoted that MOPMs with unsaturated coordination positions exposed in the pore system are preferred for the enhancement of the performance of the electrocatalytic reduction of CO₂ to alcohols. Interestingly, if the formation rates were normalized to the active Cu surface available for each MOPM, CuAdeAce showed a superior activity. This gives a clue for the design of more-efficient CO₂ reduction electrocatalysts including paddle-wheel motifs built from N-donor ligands that preserve square-planar coordination geometries around the Cu^{II} atoms and, as a result, produce open metal sites prone to interact strongly with guest molecules throughout the porous network.

Finally, the stability of the HKUST-1 GDE was confirmed for as long as 17 h of operation and can be attributed to the preservation of the local structure, even if a significant reduction in crystallinity occurred during the experimental time. These results make the use of MOPMs valuable for the electrocatalytic

conversion of CO₂ to alcohols in continuous operation. The modularity of these systems yields many opportunities for further performance improvements and open new directions in electrocatalysis.

Experimental Section

Preparation of MOPM-GDEs

Synthesis of the MOPMs: HKUST-1 was prepared by a previously described solvent-free synthetic route.^[58] In a first step, stoichiometric amounts of benzene-1,3,5-tricarboxylic acid and copper(II) acetate monohydrate were ground together to ensure a homogeneous mixture and placed in the reaction vessel. The reagent mixture was oven-heated for approximately 50 h at a heating rate of 2 °C h⁻¹ to a maximum temperature of 120 °C. Polycrystalline CuAdeAce material was prepared by the slow addition of acetic acid to an aqueous solution containing adenine and Cu^{II} salt in equimolar proportions.^[59] Both MOFs were washed thoroughly with water to remove unreacted reagents and remaining byproducts. The general procedure to prepare the MOAs (CuDTA and CuZnDTA) proceeded as follows. The corresponding metal acetate (or metal salt mixture) was dissolved in a mixture of *N,N'*-dimethylacetamide (DMA) and DMF in a 60:40 volumetric ratio, aided by an ultrasonic tip (Vibra-Cell VCX130 20 kHz and 130 W, Sonics) at 80% of its power for 2 min. Then, dithiooxamide (H₂DTA) ligand, basified with triethylamine, was dissolved in the same solvent mixture and added into the metal-ion-containing solution with the system maintained in an ultrasound bath (ULTRASONS-H, Selecta) at a temperature of 288 K. Once the metal-organic gel reached a certain consistency, it was allowed to age at room temperature for 1 d. Thereafter, the materials were washed first through immersion in pure DMF to remove the unreacted species and then by successive solvent exchanges in DMF/ethanol mixtures and pure ethanol to replace the solvent. In each exchange step, the contact between the solvent and gel was 24 h to ensure an efficient exchange. To prepare the aerogels, an E3100 critical-point dryer from Quorum Technologies equipped with gas-inlet, vent, and purge valves and a thermal bath was employed. Firstly, the gel was immersed in liquid CO₂ at 293 K and 50 bar for 1 h. After this, the exchanged ethanol was removed through the purge valve. This process was repeated five times. Subsequently, the sample was dried under supercritical conditions at a temperature of 311 K and a pressure of 85–95 bar. Finally, under constant temperature (311 K), the chamber was vented slowly to atmospheric pressure. Details on the characterization of the prepared MOPMs are provided in the Supporting Information (S2).

Preparation of the GDEs: The MOPM-GDEs were prepared by the procedure described in a previous study.^[4] The GDEs (*A* = 10 cm²) were prepared by airbrushing a catalytic ink onto a porous carbon paper (type TGP-H-60, Toray Inc.). The catalyst loading in the GDEs was kept at 1 mg cm⁻², which is an effective loading for enhanced CO₂ electrocatalytic reduction performance.^[5] The catalytic ink was formed by a mixture of the synthesized MOPMs (HKUST-1, CuAdeAce, CuDTA, and CuZnDTA) as electrocatalysts, Nafion[®] dispersion 5 wt% (Alfa Aesar) as binder, and isopropyl alcohol (IPA, Sigma-Aldrich) as the vehicle with a 70:30 catalyst/Nafion mass ratio and 3% solids (catalyst + Nafion). The mixture was sonicated for 15 min and then airbrushed onto the carbon papers, and the resulting MOPM-GDEs were dried and rinsed with deionized water before use.

Characterization of the prepared MOPM-GDEs

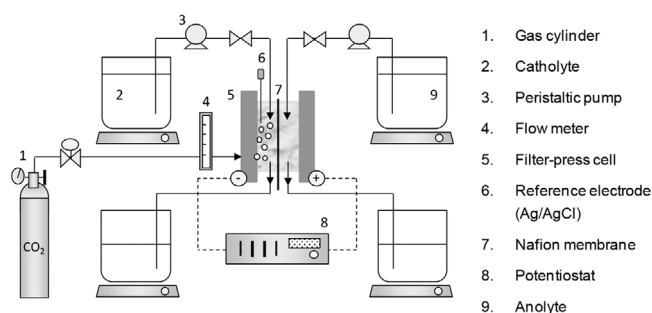
The electrochemical behavior of the materials was evaluated by cyclic voltammetry with a PGSTAT 302N potentiostat (Metrohm, Autolab B.V.) under GPES software control using a conventional three-electrode electrochemical cell. The current–voltage curves were obtained with a scan rate of 50 mV s^{-1} at potentials ranging from 0 to -1.6 V versus Ag/AgCl in a CO_2 -saturated 0.5 M KHCO_3 (Panreac) aqueous solution as the electrolyte. Portions of the MOPM-based GDEs were used as working electrodes, and glassy carbon and Ag/AgCl (sat. KCl) were used as the counter and reference electrode, respectively. The current density is expressed as the total current divided by the geometric surface area of the electrodes.

Elemental analyses (C, H, N) were performed with a Euro EA elemental analyzer (Eurovector, Milan, Italy), whereas the metal content was determined by inductively coupled plasma atomic emission spectrometry (ICP-AES) with a Horiba Yobin Yvon Activa instrument (Kyoto, Japan). The IR spectra were recorded with a Shimadzu FTIR 8400S spectrometer (Shimadzu, Kyoto, Japan) in the $4000\text{--}400 \text{ cm}^{-1}$ wavenumber region with a PIKE MIRacle universal ATR sampling accessory equipped with a ZnSe crystal. The PXRD patterns were collected using a Phillips X'PERT powder diffractometer (Panalytical, Eindhoven, The Netherlands) with $\text{CuK}\alpha$ radiation ($\lambda = 1.54060 \text{ \AA}$) over the range $5 < 2\theta < 70^\circ$ with a step size of 0.02° and an acquisition time of 2 s per step at 25°C . The N_2 (77 K) physisorption data of the materials (vacuum at 150°C for 12 h) was recorded with a Quantachrome Autosorb-iQ-MP instrument (Quantachrome Instruments, Florida, United States). Field-emission scanning electron microscopy (SEM) studies were performed with a JEOL JSM-7000F microscope. Before the analysis, all of the GDEs were coated with 5 nm of chromium.

The Cu exposure (a) of the GDEs was determined by N_2O pulse chemisorption with an AutoChem 2920 analyzer (Micromeritics, Georgia, USA) coupled to a Omnistar (Balzers Instruments, New Jersey, USA) mass spectrometer. Part of the N_2O can be reduced to N_2 and otherwise chemisorbed or left unreacted. In particular, we calculated the Cu exposure through the cumulative disappearance of N_2O . The GDEs were first treated at 100°C in a $50 \text{ cm}^3 \text{ min}^{-1}$ stream of 10 vol% H_2 in Ar (Air Liquide, Madrid, Spain) over 2 h. Then, the GDEs were kept at 35°C in a $50 \text{ cm}^3 \text{ min}^{-1}$ stream of He, and 20 pulses (0.25 cm^3 each) of 10 vol% N_2O in He (Air Liquide, Madrid, Spain) were applied. The signals of the N_2O and N_2 were recorded in the effluent by the mass spectrometer at $m/z = 44$ and 28, respectively. Cu was assumed to have a density of 1.63×10^{19} Cu atoms per m^2 .

Electrochemical cell and experimental conditions

The prepared MOPM-GDEs were evaluated for the continuous electrocatalytic reduction of CO_2 in a filter-press electrochemical cell (Micro Flow Cell, ElectroCell A/S) under ambient conditions. A Nafion 117 cation-exchange membrane was used to separate the cathode and anode compartments. The MOPM-GDEs were employed together with a platinumized titanium electrode as the anode and a Ag/AgCl (sat. KCl) reference electrode assembled close to the cathode. A schematic representation of the experimental plant is shown in Scheme 1. The cathode side of the reactor was fed with CO_2 gas (99.99%) at $Q_g/A = 10$ to $40 \text{ mL min}^{-1} \text{ cm}^{-2}$. A 0.5 M KHCO_3 (Panreac) aqueous solution was used as both the catholyte and anolyte at $Q_l/A = 1\text{--}4 \text{ mL min}^{-1} \text{ cm}^{-2}$. The electrolytes were pumped from the catholyte and anolyte tanks to the cell by two



Scheme 1. Schematic representation of the experimental setup.

peristaltic pumps (Watson Marlow 320, Watson Marlow Pumps Group). In this study, the filter-press electrochemical system possesses three inputs (catholyte, anolyte, and CO_2 separately) and two outputs (catholyte- CO_2 and anolyte), which make possible the formation of a gas–solid–liquid interface for the electrocatalytic reduction of CO_2 in the gas phase.^[4]

All of the experiments were performed under galvanostatic conditions (i.e., at a constant current density) with an AutoLab PGSTAT 302N potentiostat (Metrohm, Autolab B.V.). The current density ranged from $j = 5$ to 40 mA cm^{-2} . The experimental time was 90 min, for which pseudostable conditions are ensured according to our previous analyses.^[4,5] Liquid samples were taken every 15 min from the catholyte tank. To quantify the concentration of each product in the liquid phase, the samples were analyzed in duplicate in a headspace gas chromatograph (GC–MS QP2010, Ultra Shimadzu) equipped with a flame ionization detector (FID). The compounds were separated using a DB-Wax $30 \text{ m} \times 0.25 \text{ mm} \times 0.25 \text{ }\mu\text{m}$ column with an injection and detector temperature of 250 and 270°C , respectively. Helium was used as the carrier gas at a flow rate of 50 mL min^{-1} . The identification of the obtained products was further confirmed by a headspace GC–MS instrument (N5975B) equipped with a $60 \text{ m} \times 250 \text{ }\mu\text{m} \times 1.40 \text{ }\mu\text{m}$ DB-624 capillary column. The product concentrations were averaged from at least three replicates. The standard deviations of all experiments were below 19.2%.

The performance of the electrochemical processes were evaluated through the rate of product formation, r (i.e., the product obtained per unit of cathode area and time), and the Faradaic efficiency, FE (i.e., the selectivity of the reaction for the formation of the different products), according to Equation (1):

$$\text{FE}(\%) = (znF)/q \times 100 \quad (1)$$

z is the theoretical number of electrons exchanged to form the desired product, n is the number of moles produced, F is the Faradaic constant (96485 C mol^{-1}), and q is the total charge applied in the process.

Acknowledgements

The authors gratefully acknowledge the financial support from the Spanish Ministry of Economy and Competitiveness (MINECO) under projects CTQ2013-48280-C3-1-R and CTQ2013-48280-C3-3-R and MAT2013-46502-C2-1-P, and the Juan de la Cierva program (JCI-2012-12073).

Keywords: alcohols · copper · electrodes · metal–organic frameworks · reduction

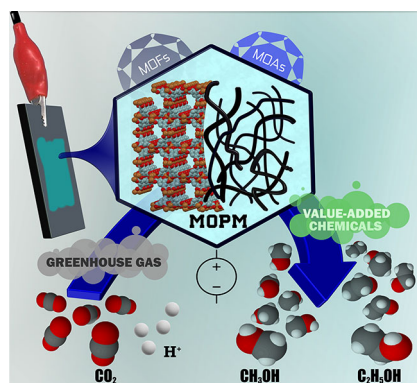
- [1] M. E. Boot-Handford, J. C. Abanades, E. J. Anthony, M. J. Blunt, S. Brandani, N. Mac Dowell, J. R. Fernandez, M. C. Ferrari, R. Gross, J. P. Hallet, R. S. Haszeldine, P. Heptonstall, A. Lyngfelt, Z. Makuch, E. Mangano, R. T. J. Porter, M. Pourkashanian, G. T. Rochelle, N. Shah, J. G. Yao, P. S. Fenell, *Energy Environ. Sci.* **2014**, *7*, 130–189.
- [2] J. Albo, T. Yoshioka, T. Tsuru, *Sep. Purif. Technol.* **2014**, *122*, 440–448.
- [3] J. Albo, A. Irabien, *J. Chem. Technol. Biotechnol.* **2012**, *87*, 1502–1507.
- [4] J. Albo, A. Irabien, *J. Catal.* **2015**, DOI: 10.1016/j.jcat.2015.11.014.
- [5] J. Albo, A. Sáez, J. Solla-Gullón, A. Irabien, *Appl. Catal. B* **2015**, *176*–177, 709–717.
- [6] A. Del Castillo, M. Alvarez-Guerra, A. Irabien, *AIChE J.* **2014**, *60*, 3557–3564.
- [7] G. Centi, S. Perathoner, *Catal. Today* **2009**, *148*, 191–205.
- [8] J. Albo, M. Alvarez-Guerra, P. Castaño, A. Irabien, *Green Chem.* **2015**, *17*, 2304–2324.
- [9] J. Qiao, Y. Liu, F. Hong, J. Zhang, *Chem. Soc. Rev.* **2014**, *43*, 631–675.
- [10] M. Alvarez-Guerra, J. Albo, E. Alvarez-Guerra, A. Irabien, *Energy Environ. Sci.* **2015**, *8*, 2574–2599.
- [11] I. Ganesh, *Renewable Sustainable Energy Rev.* **2014**, *31*, 221–257.
- [12] A. Goepfert, M. Czaun, J. P. Jones, G. K. Surya Prakash, G. A. Olah, *Chem. Soc. Rev.* **2014**, *43*, 7995–8048.
- [13] M. Gattrell, N. Gupta, A. Co, *J. Electroanal. Chem.* **2006**, *594*, 1–19.
- [14] A. A. Peterson, F. Abild-Pedersen, F. Studt, J. Rossmeisl, J. K. Nørskov, *Energy Environ. Sci.* **2010**, *3*, 1311–1315.
- [15] K. P. Kuhl, E. R. Cave, D. N. Abram, T. F. Jaramillo, *Energy Environ. Sci.* **2012**, *5*, 7050–7059.
- [16] Y. Liu, Z. U. Wang, H. C. Zhou, *Greenhouse Gases Sci. Technol.* **2012**, *2*, 239–259.
- [17] J. Gascon, A. Corma, F. Kapteijn, F. X. Llabrés I Xamena, *ACS Catal.* **2014**, *4*, 361–378.
- [18] A. Doménech, H. García, M. T. Doménech-Carbó, F. Llabrés-i-Xamena, *J. Phys. Chem. C* **2007**, *111*, 13701–13711.
- [19] R. S. Kumar, S. S. Kumar, M. A. Kulandainathan, *Electrochem. Commun.* **2012**, *25*, 70–73.
- [20] R. Hinogami, S. Yotsuhashi, M. Deguchi, Y. Zenitani, H. Hashiba, Y. Yamada, *ECS Electrochem. Lett.* **2012**, *1*, H17–H19.
- [21] T. Maihom, S. Wannakao, B. Boekfa, J. Limtrakul, *J. Phys. Chem. C* **2013**, *117*, 17650–17658.
- [22] I. Hod, P. Deria, W. Bury, J. E. Mondloch, C. W. Kung, M. So, M. D. Sampson, A. W. Peters, C. P. Kubiak, O. K. Farha, J. R. Hupp, *Nat. Commun.* **2015**, *6*, 8304.
- [23] I. Hod, M. D. Sampson, P. Deria, C. P. Kubiak, O. K. Farha, J. T. Hupp, *ACS Catal.* **2015**, *5*, 6302–6309.
- [24] N. Kornienko, Y. Zhao, C. S. Kley, C. Zhu, D. Kim, S. Lin, C. J. Chang, O. M. Yaghi, P. Yang, *J. Am. Chem. Soc.* **2015**, *137*, 14129–14135.
- [25] W. Xia, A. Mahmood, R. Zou, Q. Xu, *Energy Environ. Sci.* **2015**, *8*, 1837–1866.
- [26] S. Lin, C. S. Diercks, Y. B. Zhang, N. Kornienko, E. M. Nichols, Y. Zhao, A. R. Paris, D. Kim, P. Yang, O. M. Yaghi, C. J. Chang, *Science* **2015**, *349*, 1208–1213.
- [27] M. R. Lohe, M. Rose, S. Kaskel, *Chem. Commun.* **2009**, 6056–6058.
- [28] S. Xiang, L. Li, J. Zhang, X. Tan, H. Cui, J. Shi, Y. Hu, L. Chen, C. Y. Su, S. L. James, *J. Mater. Chem.* **2012**, *22*, 1862–1867.
- [29] L. Li, S. Xiang, S. Cao, J. Zhang, G. Ouyang, L. Chen, C. Y. Su, *Nat. Commun.* **2013**, *4*, 1174.
- [30] Q. Yang, X. Tan, S. Wang, J. Zhang, L. Chen, J. P. Zhang, C. Y. Su, *Microporous Mesoporous Mater.* **2014**, *187*, 108–113.
- [31] H. Zhu, X. Yang, E. D. Cranston, S. Zhu, *Adv. Mater.* **2016**, DOI: 10.1002/adma.201601351.
- [32] S. S. Chui, S. M. Lo, J. P. Charmant, A. G. Orpen, I. D. Williams, *Science* **1999**, *283*, 1148–1150.
- [33] K. Sumida, D. L. Rogow, J. A. Mason, T. M. McDonald, E. D. Bloch, Z. R. Herm, T. Bae, J. R. Long, *Chem. Rev.* **2012**, *112*, 724–781.
- [34] S. Pérez-Yáñez, G. Beobide, O. Castillo, M. Fischer, F. Hoffmann, M. Fröba, J. Cepeda, A. Luque, *Eur. J. Inorg. Chem.* **2012**, 5921–5933.
- [35] T. Y. Chang, R. M. Liang, P. W. Wu, J. Y. Chen, Y. C. Hsieh, *Mater. Lett.* **2009**, *63*, 1001–1003.
- [36] M. Le, M. Ren, Z. Zhang, P. T. Sprunger, R. L. Kurtz, J. C. Flake, *J. Electrochem. Soc.* **2011**, *158*, E45–E49.
- [37] Y. Lan, S. Ma, J. Lu, P. J. A. Kenis, *Int. J. Electrochem. Sci.* **2014**, *9*, 7300–7308.
- [38] F. Jia, X. Yu, L. Zhang, *J. Power Sources* **2014**, *252*, 85–89.
- [39] D. Chi, H. Yang, Y. Du, T. Lv, G. Sui, H. Wang, J. Lu, *RSC Adv.* **2014**, *4*, 37329–37332.
- [40] R. Kas, R. Kortlever, A. Milbrat, M. T. M. Koper, G. Mul, J. Baltrusaitis, *Phys. Chem. Chem. Phys.* **2014**, *16*, 12194–12201.
- [41] C. W. Li, J. Ciston, M. W. Kanan, *Nature* **2014**, *508*, 504–507.
- [42] D. Ren, Y. Deng, A. D. Handoko, C. S. Chen, S. Malkhandi, B. S. Yeo, *ACS Catal.* **2015**, *5*, 2814–2821.
- [43] R. Kas, R. Kortlever, H. Yilmaz, T. M. Koper, G. Mul, *ChemElectroChem* **2015**, *2*, 354–358.
- [44] C. Genovese, C. Ampelli, B. C. Marepally, G. Papanikolaou, S. Perathoner, G. Centi, *Chem. Eng. Trans.* **2015**, *43*, 2281–2286.
- [45] A. Javier, J. H. Baricuatro, Y. G. Kim, M. P. Soriaga, *Electrocatalysis* **2015**, *6*, 493–497.
- [46] N. Gutiérrez-Guerra, L. Moreno-López, J. C. Serrano-Ruiz, J. L. Valverde, A. de Lucas-Consuegra, *Appl. Catal. B* **2016**, *188*, 272–282.
- [47] Q. Wang, H. Dong, H. Yu, *RSC Adv.* **2014**, *4*, 59970–59976.
- [48] Q. Wang, H. Dong, H. Yu, *J. Power Sources* **2014**, *271*, 278–284.
- [49] J. Wu, P. P. Sharma, B. H. Harris, X. D. Zhou, *J. Power Sources* **2014**, *258*, 189–194.
- [50] S. Lee, H. Ju, R. Machunda, S. Uhm, J. Kwang Lee, H. Jin Lee, J. Lee, *J. Mater. Chem. A* **2015**, *3*, 3029–3034.
- [51] K. W. Frese, *J. Electrochem. Soc.* **1991**, *138*, 3338–3344.
- [52] L. M. Aeshala, R. G. Uppaluri, A. Verma, *J. CO₂ Util.* **2013**, *3–4*, 49–55.
- [53] E. Andrews, M. Ren, F. Wang, Z. Zhang, P. Sprunger, R. Kurtz, J. Flake, *J. Electrochem. Soc.* **2013**, *160*, H841–H846.
- [54] D. P. Summers, S. Leach, K. W. Frese, *J. Electroanal. Chem.* **1986**, *205*, 219–232.
- [55] A. Li, H. Wang, J. Han, L. Liu, *Front. Chem. Sci. Eng.* **2012**, *6*, 381–388.
- [56] L. M. Huang, H. T. Wang, J. X. Chen, Z. B. Wang, J. Y. Sun, D. Y. Zhao, Y. S. Yan, *Microporous Mesoporous Mater.* **2003**, *58*, 105–114.
- [57] S. Hausdorf, J. Wagler, R. Mossig, F. O. Mertens, *J. Phys. Chem. A* **2008**, *112*, 7567–7576.
- [58] M. Lanchas, S. Arcediano, A. T. Aguayo, G. Beobide, O. Castillo, J. Cepeda, D. Vallejo-Sánchez, A. Luque, *RSC Adv.* **2014**, *4*, 60409–60412.
- [59] S. Pérez-Yáñez, G. Beobide, O. Castillo, J. Cepeda, A. Luque, A. T. Aguayo, P. Román, *Inorg. Chem.* **2011**, *50*, 5330–5332.

Received: May 24, 2016

Published online on ■■■■■, 0000

FULL PAPERS

Closing the loop: Metal–organic porous materials are effective electrocatalysts for the continuous electrochemical conversion of CO₂ to alcohols, a process that could promote the transition to a low-carbon economy. The modularity of these systems yields many opportunities for further performance improvements and opens new directions in electrocatalysis.



J. Albo, D. Vallejo, G. Beobide,
O. Castillo, P. Castaño, A. Irabien*



**Copper-Based Metal–Organic Porous
Materials for CO₂ Electrocatalytic
Reduction to Alcohols**

